AIAA SciTech
13-17 January 2014, National Harbor, Maryland
55th AIAA/ASMe/ASCE/AHS/SC Structures, Structural Dynamics, and Materials Conference

Nonintrusive Reduced Order Modeling for the Nonlinear Geometric Response of Some Joined Wings

Greg Phlipot[1], X.Q. Wang[2], and Marc P. Mignolet[3]
SEMTE, Faculties of Mechanical and Aerospace Engineering, Arizona State University, Tempe, AZ, 85287, USA

Luciano Demasi[4] and Rauno Cavallaro[5]
Department of Mechanical and Aerospace Engineering, San Diego State University, San Diego, CA, 92182, USA

Abstract

The focus of this investigation is on assessing the use of nonintrusive (i.e. developed directly from commercial finite element codes) nonlinear reduced order modeling techniques for the prediction of the strongly nonlinear response of joined wings, e.g. the snap-buckling they exhibit. A key component of the reduced order modeling is the selection of the basis to represent the response and this aspect will be extensively discussed leading to the formulation of new metrics for the assessment of the basis. The reduced order models constructed with bases satisfying these metrics performed well in capturing the strongly nonlinear events in comparison to the predictions of the finite element code from which they are derived.

I. Introduction

Joined wings have received considerable attention recently owing in particular to the Boeing Sensor-Craft design, see Fig. 1, but they have been considered for a much longer time, e.g. see the 1986 review paper [1]. The joining of the wings, either as in the Boeing Sensor-Craft design of Fig. 1 or in the PrandtlPlane-like [2] concept (box wing) of Fig. 2, provides a significant increase in stiffness (closed system) as compared to single wing models and thus is typically proposed for long and slender wings. Note that the coupling of the wings by the joint occurs in all directions, i.e. for both transverse and inplane displacements, and the positive effect achieved in the transverse direction (increase in stiffness) may be countered by the possible occurrence of buckling and snap through response resulting from the inplane coupling.

A surprising feature of this wing is that even, far from the snap-instability and for small deformations, the response may be already nonlinear. The conceptual studies of [3,4] provide a detailed perspective on the physical behavior of the wings. It was in particular shown that the typical snap behavior exhibited at macrogeometrical level may not be explained through the classical loading arguments (Euler beam). This discrepancy is confirmed by the inability of linear stability tools to predict the real critical load.

Further, linearized tools may also be misleading on how to increase the buckling load. An intuitive approach to achieve this task is, as for example to increase the stiffness of the wing under compression, resulted in having actually the opposite effect [4].

---

[1] Undergraduate Research Assistant
[2] Associate Research Scientist, Senior Member AIAA
[3] Professor, Associate Fellow AIAA
[4] Associate Professor, Member AIAA
[5] Graduate Research Assistant

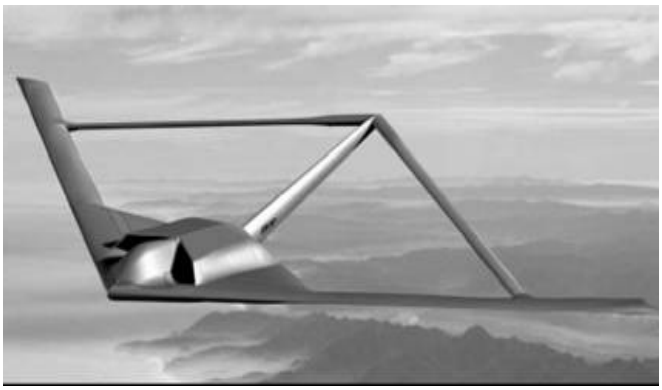

Figure 1. Boeing Sensor-Craft Concept.

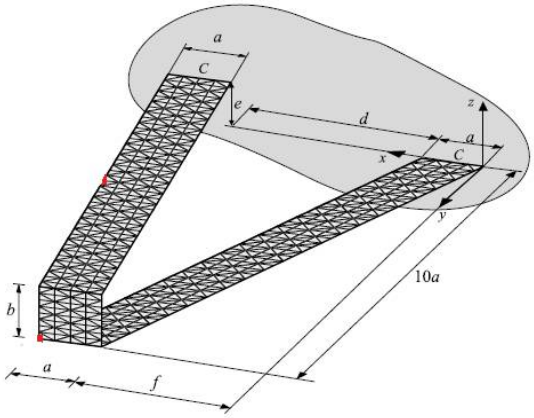

Figure 2. PrandtlPlane concept [2].

The characteristic physics inherent to this phenomenon has been partly discussed in [4]. Among them, it was shown that the lower-to-upper-wing bending stiffnesses ratio was one of the major parameters driving the instability. However, when torsion-bending coupling were important, it was not possible to clearly draw more general conclusions [4].

As a final note, the overconstrained nature of the system represents a limit to efforts to understand the physics with a "local" approach consisting in a conceptual isolation of portions of the system.

Clearly, nonlinear finite element codes, e.g. Abaqus and Nastran for commercial codes, can be used to achieve the necessary nonlinear structural modeling. Their use is however computationally much more demanding than in the linear case and renders significantly more challenging the coupling with any aerodynamic code for the prediction of the aeroelastic response of the wing. A particularly convenient approach to resolve these difficulties while maintaining an accurate modeling of the nonlinear effects is to rely on a modal-like reduced order model of the structural response such as those reviewed recently in [5] which are derived from standard commercial finite element codes. The focus of the present paper is on demonstrating and validating the construction of such nonlinear ROMs, specifically those following [6-8], for several structural models including configurations of the PrandtlPlane as a first step toward the aeroelastic study of these wings.

II. Reduced Order Model Background

A. Reduced Order Model Equations

The reduced order models (ROM) considered here are based on a representation of the nonlinear geometric response of the structure in the form

$$\underline{u}(t) = \sum_{n=1}^{M} q_n(t)\, \underline{\psi}^{(n)} \tag{1}$$

where, $\underline{u}(t)$ denotes the vector of displacements of the finite element degrees of freedom and $\underline{\psi}^{(n)}$ are specified, constant basis functions. Under appropriate conditions, see [5,6], the

governing equations for the time dependent generalized coordinates $q_n(t)$ may be expressed as

$$M_{ij}\ddot{q}_j + D_{ij}\dot{q}_j + K_{ij}^{(1)}\, q_j + K_{ijl}^{(2)} q_j q_l + K_{ijlp}^{(3)} q_j q_l q_p = F_i \qquad (2)$$

Note in Eq. (2) that a linear damping term $D_{ij}\,\dot{q}_j$ has been added to collectively represent various dissipation mechanisms. Further, M_{ij} denotes the elements of the mass matrix, $K_{ij}^{(1)}$, $K_{ijl}^{(2)}$, $K_{ijlp}^{(3)}$ are linear, quadratic, and cubic stiffness coefficients and F_i are the modal forces.

A key condition on the derivation of Eq. (2) is that elasticity be defined as a linear relation between the strain and stress tensors of a *total* Lagrangian formulation, i.e. between the Green strain and 2nd Piola-Kirchhoff stress tensors. This assumption is however not the one introduced in Nastran plates and beam models which is carried out in an *updated* Lagrangian framework and with associated tensors. This issue has been recognized in prior studies, e.g. in [8,9], in which it was found that the reduced order model predictions match well those of Nastran for peak displacements up to 15% or so of span. It is accordingly in this range of displacements that the joined wings will be studied.

B. Reduced Order Model Basis Selection

One of the key challenges in the construction of a good reduced order model is in the selection of the basis functions $\underline{\psi}^{(n)}$; if the structural response is not well represented within this basis, the corresponding prediction of the reduced order model will in general be poor. The modes/basis functions needed for a nonlinear problem are certainly expected to include those used for the corresponding linear problem, but others are also anticipated to model the difference in physical behavior induced by the nonlinearity not directly by the loading.

This issue was addressed in [6-8] through the inclusion in the basis of an additional set of basis functions referred to as dual modes aimed at these nonlinear effects. The key idea in this approach is to first subject the structure to a series of "representative" static loadings, and determine the corresponding *nonlinear* displacement fields. Then, extract from them additional basis functions, the "dual modes", to append to the linear basis, i.e. the modes that would be used in the linear case. It was argued in [6] that the representative static loadings should be selected to excite primarily the linear basis modes and, in fact, in the absence of geometric nonlinearity (i.e. for a linear analysis) should only excite these modes. That is, the applied load vectors $\underline{F}_{FE}^{(m)}$ on the structural finite element model should be such that the corresponding linear static responses are of the form

$$\underline{u}^{(m)} = \sum_i \alpha_i^{(m)}\ \underline{\psi}^{(i)} \qquad (3)$$

which occurs when

$$\underline{F}_{FE}^{(m)} = \sum_i \alpha_i^{(m)}\, K_{FE}^{(1)}\, \underline{\psi}^{(i)} \qquad (4)$$

where $\alpha_i^{(m)}$ are coefficients to be chosen with *m* denoting the load case number. A detailed discussion of the linear combinations to be used is presented in [6] but, in all validations carried out, it has been sufficient to consider the cases

$$\underline{F}_{FE}^{(m)} = \alpha_i^{(m)} K_{FE}^{(1)} \underline{\psi}^{(i)} \quad i = \text{dominant mode} \tag{5}$$

and

$$\underline{F}_{FE}^{(m)} = \frac{\alpha_i^{(m)}}{2} K_{FE}^{(1)} \left[\underline{\psi}^{(i)} + \underline{\psi}^{(j)} \right] \quad i = \text{dominant mode}, \; j \neq i \tag{6}$$

where a "dominant" mode is loosely defined as one expected to provide a large component of the structural response to the physical loading. The ensemble of loading cases considered is formed by selecting several values of $\alpha_i^{(m)}$ for each dominant mode in Eq. (5) and also for each mode $j \neq i$ in Eq. (6). Note further that both positive and negative values of $\alpha_i^{(m)}$ are suggested and that their magnitudes should be such that the corresponding displacement fields $\underline{u}^{(m)}$ range from near linear cases to some exhibiting a strong nonlinearity.

The next step of the basis construction is the extraction of the nonlinear effects in the obtained displacement fields, which is achieved by removing from the displacements fields their projections on the linear basis. Finally, a proper orthogonal decomposition (POD) analysis of each set of "nonlinear responses" is then sequentially carried out to extract the dominant features of these responses which are then selected as dual modes, see [6] for full details.

An assessment of the applicability of a particular basis for a specific problem can be carried out from a set of representative full finite element responses $\underline{u}$ by quantifying the difference between these responses and their projections on the basis. To this end, introduce the representation error defined as

$$\varepsilon_{rep} = \frac{\left\| \underline{u} - \underline{u}_{proj} \right\|}{\left\| \underline{u} \right\|} \tag{7}$$

where $\underline{u}_{proj}$ is the projection of $\underline{u}$ on the basis. For ε_{rep} small enough, typically below 1% on all translations degrees of freedom, the basis may be expected to be appropriate for the representation of the full finite element model nonlinear response.

C. Identification of Reduced Order Model Parameters

The identification of the ROM parameters is the process by which the stiffness coefficients of Eq. (2) are determined using the commercial (Nastran here) finite element model of the structure and the basis functions $\underline{\psi}^{(n)}$. Several strategies are possible to accomplish this task (see [5] for review) but the procedure recently derived in [7] will be used here. This approach relies on the availability of the final *tangent stiffness matrix* of the structure under an imposed displacement and is briefly reviewed below.

The *iu* component of the reduced order tangent stiffness matrix can be derived from the cubic stiffness operator of Eq. (2) as

$$\begin{aligned} K_{iu}^{(T)} &= \frac{\partial}{\partial q_u}\left[K_{ij}^{(1)}\, q_j + K_{ijl}^{(2)} q_j q_l + K_{ijlp}^{(3)} q_j q_l q_p\right] \\ &= K_{iu}^{(1)} + \left[K_{iju}^{(2)} + K_{iuj}^{(2)}\right] q_j + \left[K_{ijlu}^{(3)} + K_{ijul}^{(3)} + K_{iujl}^{(3)}\right] q_j q_l \end{aligned} \tag{8}$$

The stiffness coefficients $K_{ij}^{(1)}$, $K_{ijl}^{(2)}$, and $K_{ijlp}^{(3)}$ can then be determined by imposing the matching, for a series of deformed configurations, of the reduced order tangent stiffness matrix with the projection on the basis of its finite element counterpart $\hat{K}^{(T)}$. That is,

$$K^{(T)}(\underline{q}^{(p)}) = \Psi^T \hat{K}^{(T)}(\underline{u}^{(p)})\,\Psi \quad \text{where } \underline{u}^{(p)} = \Psi \underline{q}^{(p)} \tag{9}$$

for a series of p = 1, ..., P deformed configurations. In the above equations, the subscript ^{T} denotes the operation of matrix transposition and Ψ is the modal matrix

$$\Psi = \left[\underline{\psi}^{(1)}\ \underline{\psi}^{(2)} \ldots \underline{\psi}^{(M)}\right] \ . \tag{10}$$

The deformed configurations $\underline{u}^{(p)} = \Psi \underline{q}^{(p)}$ selected here are those of the imposed displacement scheme (see [5,6]). Consider first the situation in which the imposed displacement is along a single basis function, i.e. $\underline{u} = q_j\ \underline{\psi}^{(j)}$. The corresponding ROM tangent stiffness matrix can then be written as (no sum on *i*)

$$K_{iu}^{(T)} = K_{iu}^{(1)} + \left[K_{iju}^{(2)} + K_{iuj}^{(2)}\right] q_j + \left[K_{ijju}^{(3)} + K_{ijuj}^{(3)} + K_{iujj}^{(3)}\right] q_j^2 \tag{11}$$

Since the elements $K_{ijl}^{(2)}$ and $K_{ijlp}^{(3)}$ may be selected as zero unless $p \geq l \geq j$, the above equation is equivalent to

$$K_{iu}^{(T)} = \left[\Psi^T \hat{K}^{(T)} \Psi\right]_{iu} = K_{iu}^{(1)} + K_{iju}^{(2)} q_j + K_{ijju}^{(3)} q_j^2 \qquad j < u \tag{12}$$

$$K_{iu}^{(T)} = \left[\Psi^T \hat{K}^{(T)} \Psi\right]_{iu} = K_{iu}^{(1)} + 2\,K_{iuu}^{(2)} q_u + 3\,K_{iuuu}^{(3)}\, q_u^2 \qquad j = u \tag{13}$$

$$K_{iu}^{(T)} = \left[\Psi^T \hat{K}^{(T)} \Psi\right]_{iu} = K_{iu}^{(1)} + K_{iuj}^{(2)} q_j + K_{iujj}^{(3)} q_j^2 \qquad j > u \tag{14}$$

from which the coefficients $K_{ijl}^{(2)}$, $K_{ijjl}^{(3)}$, and $K_{ijll}^{(3)}$ can be estimated if it is assumed that the linear stiffness coefficients are obtained as in linear modal analyses.

The final step in the identification of the reduced order model is to evaluate the coefficients

$K_{ijlu}^{(3)}$ for $j \neq l$, $j \neq u$, and $u \neq l$. They can be evaluated from the knowledge of $K_{iu}^{(T)}$ corresponding to a displacement field which involves both basis functions j and l, i.e. of the form of $\underline{u} = q_n \ \underline{\psi}^{(n)} + q_m \ \underline{\psi}^{(m)}$. Then, $K_{iu}^{(T)}$ is given by Eq. (3) in which no summation on j and l applies. Specifically, for $u > l > j$, one has

$$K_{iu}^{(T)} = \left[\Psi^T \hat{K}^{(T)} \Psi\right]_{iu} = K_{iu}^{(1)} + \left[K_{iju}^{(2)} \ q_j + K_{ilu}^{(2)} \ q_l\right] + \left[K_{ijlu}^{(3)} \ q_j \ q_l + K_{ijju}^{(3)} \ q_j^2 + K_{illu}^{(3)} \ q_l^2\right] \tag{15}$$

in which all terms are known except $K_{ijlu}^{(3)}$.

Note in the above procedure that only combinations of two modes are used and thus the number of deformed configurations to consider is only of order $O\left(M^2\right)$, it is indeed $2M + M\left(M-1\right)/2$.

D. ROM Application for Monotonic Nonlinearity

The ROM methodology described in the previous section has been applied to a number of structural models, e.g. see [6-11], most of which exhibiting a "monotonic" nonlinearity, i.e. a stiffening of the system which increases with increasing deformation/load level. This nonlinearity could be strong, as in fully clamped structures, or rather weak, as observed for several cantilevered structures. In these various cases, the strategy described in the previous sections, with only occasional minor adjustments, has led to a reduced order model providing a very close fit of full finite element predictions. The aluminum plate of Fig. 3 is an example of such situations. It is reinforced along its edges by an aluminum beam and supported at its four corners only (see [6] for details) while subjected to a uniform pressure of constant direction. A 12 transverse - 12 duals (based on mode 1 dominant, see Section II.B) basis was constructed and led to the representation errors vs. applied pressure seen in Fig. 4. Based on these rather low representation errors, the coefficients of the 24-mode ROM were evaluated and the corresponding ROM responses to the uniform pressure computed. The comparison of the transverse displacements of the plate center predicted by the ROM and by the full Nastran model is shown in Fig. 5. Clearly, the matching is excellent.

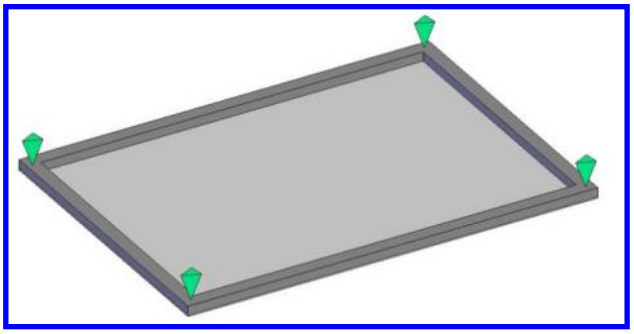

Figure 3. Beam stiffened plate supported at its four corners.

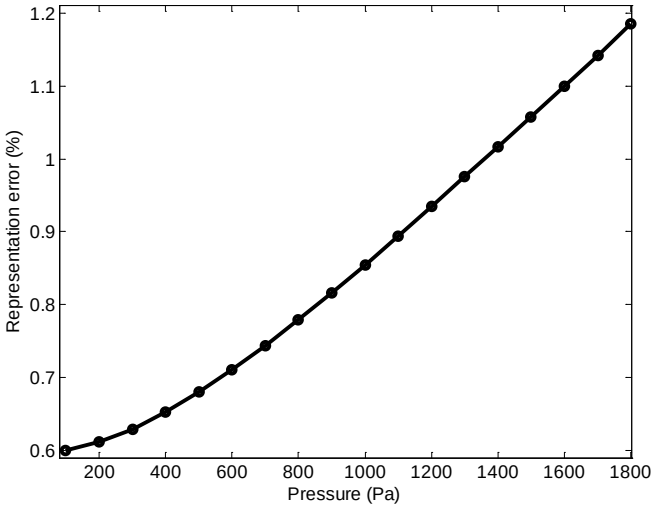

Figure 4. Representation error ε_{rep} of the beam stiffened plate displacement fields as a function of the uniform load magnitude.

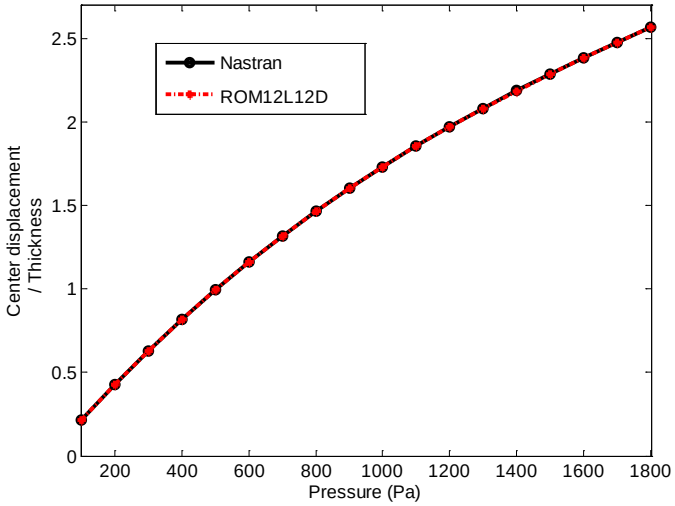

Figure 5. Transverse displacement of the beam stiffened plate center predicted by both the reduced order model and the full finite element model.

III. ROM Application to a Structure with Snap-Through

Structures exhibiting non-monotonic nonlinearity have also been considered in past applications of the present reduced order modeling strategy but to a smaller extent than those with monotonic nonlinearity. One key example is the clamped-clamped curved beam of Fig. 6 (see [5,10,11] and references therein) which has an elastic modulus of 10.6×10^{6} psi, shear modulus of 4.0×10^{6} psi, and density of 2.588×10^{-4} lbf-sec^2/in^4. A Nastran finite element model of this beam was developed with 144 beam (CBEAM) elements which permitted a baseline static analysis of the beam under the uniform load of constant direction shown in Fig. 6. It was in particular found that the beam exhibits an antisymmetric snap-through at the pressure of 1.89 lb/in and a symmetric one at 2.3lb/in if the antisymmetric one is blocked.

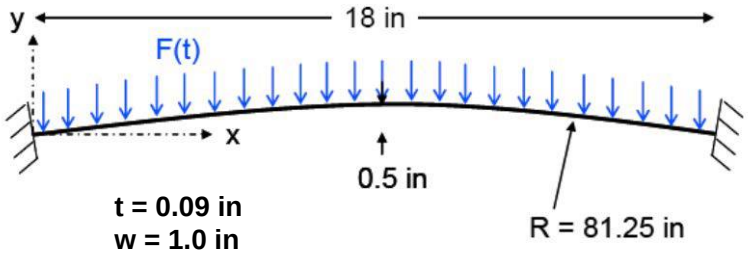

Figure 6. Clamped-clamped curved beam geometry.

Reduced order models of this structure, extending past the snap-through occurrences, have been successfully developed with the methodology of section 2 in [10,11]. Of primary interest here is the purely symmetric response and snap-through, see Fig. 7 for the load-displacement curve of the vertical displacement of the beam center as predicted by Nastran. Also shown on this figure, are the predictions obtained with two reduced order models constructed from the first symmetric modes of the beam and the corresponding duals with mode 1 dominant. As suggested in section II.B, the magnitude of the coefficients $\alpha_i^{(m)}$ was selected so that the resulting displacement fields $\underline{u}^{(m)}$ encompass the entire range of behaviors, i.e. from linear to post snap-through response. The first of the two ROMs used only the first 4 linear modes and 4 corresponding duals (the 4L4D model) while the second one involved 6 linear modes and 7 corresponding duals (the 6L7D model).

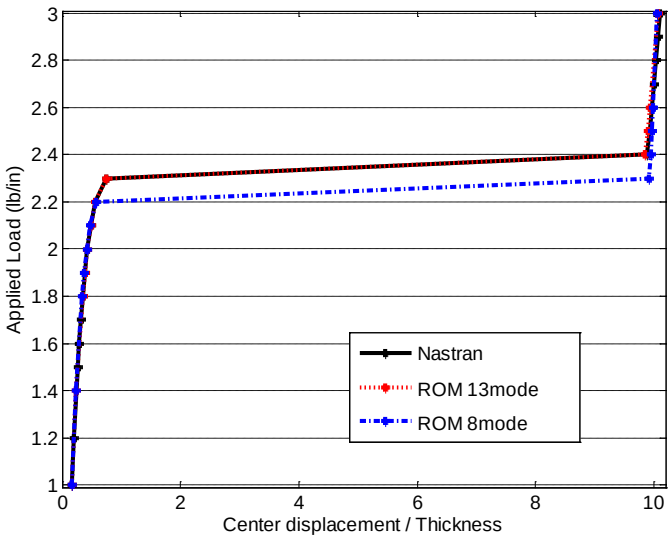

Figure 7. Clamped-clamped curved beam load-displacement curve of the vertical displacement of the beam center obtained by Nastran and two reduced order models.

The representation errors of these two bases are shown in Fig. 8(a) and (b), respectively. The 4L4D model is characterized by representation errors which are of the same magnitude as those in Fig. 4. However, the larger reduced order model (6L7D) has errors typically 5 times smaller than those of the 4L4D model.

With representation errors below 0.5%, both of these bases appeared to be at least acceptable and thus their associated stiffness coefficients were evaluated and the corresponding responses

under an increasing applied load determined. The results of this effort are shown in Fig. 7 and it is seen that the 13-mode model (6L7D) provides an excellent approximation of the Nastran predictions, including the snap-through load and post snap-through behavior. The 4L4D model also performs well away from the snap-through load condition but not very near it, the predicted snap-through load is 2.2 vs. 2.3.

These results suggest that the capturing of the snap-through load condition correctly may require a better model than what would be required to predict the response away from this condition. This finding is in fact quite reasonable: the occurrence of a snap-through results from an eigenvalue of the tangent stiffness matrix becoming zero. This is a rather stringent condition on the ROM as (i) the tangent stiffness matrix is expected to be less well matched by the ROM than the forces as it is a derivative of these forces and (ii) the location of the zero may easily shift with small changes in coefficients.

This discussion suggests that two additional checks of the basis be conducted. The first one involves the representation of the lowest eigenvector of the tangent stiffness matrix while the second focuses on assessing the capability of the basis to capture the zero of the eigenvalue. The first check, i.e. the representation error of the first eigenvector of the tangent stiffness matrix, is presented in Fig. 8 for the two ROMs. It is seen that this representation error is typically larger than the one of the response (as is suggested above) but that it exhibits the same trends as its counterpart for the response.

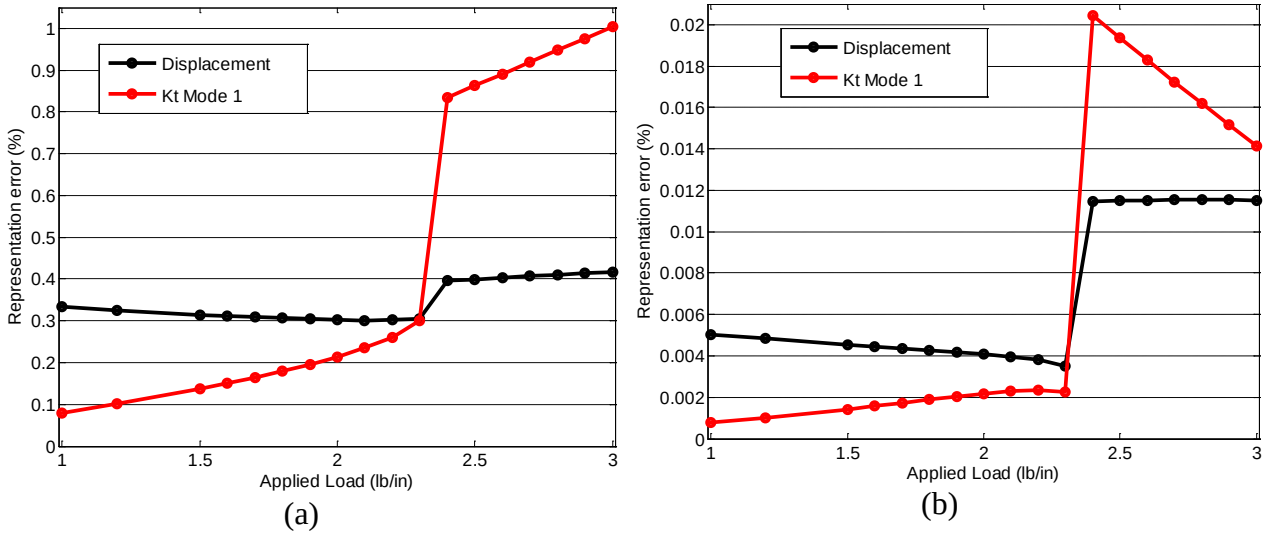

Figure 8. Representation errors ε_{rep} of the displacements under uniform load and of the first eigenvector of the corresponding tangent stiffness matrix. Clamped-clamped curved beam (a) ROM 4L4D (b) ROM 6L7D.

The second of the above additional checks, i.e. the assessment of the capability of the basis to predict a snap-through, can be carried out as follows. First, determine the full finite element tangent stiffness matrix for a set of loading conditions including the snap-through. Then, project this matrix on the basis, e.g. as in Eq. (15). Finally, proceed with the computation of the lowest eigenvalue of this matrix. The results of this check are presented in Fig. 9 for both 4L4D and 6L7D basis. It is seen that both reduced order bases do provide a good capture of the zero eigenvalue. However, the lowest eigenvalue of the reduced order model (with identified coefficients) does not perform as well for the smaller ROM (4L4D). This issue does not arise

from the identification of the stiffness coefficients as they are the same for the 8 common modes of the two models. Rather, it must come from the added flexibility of the representation provided by the additional 5 modes of the larger ROM or, somewhat equivalently, from the better representation of the eigenvector associated with this eigenvalue, see Figs 8(a) and (b).

These newly proposed validation metrics provide enhanced guidelines for the selection of the ROM basis .

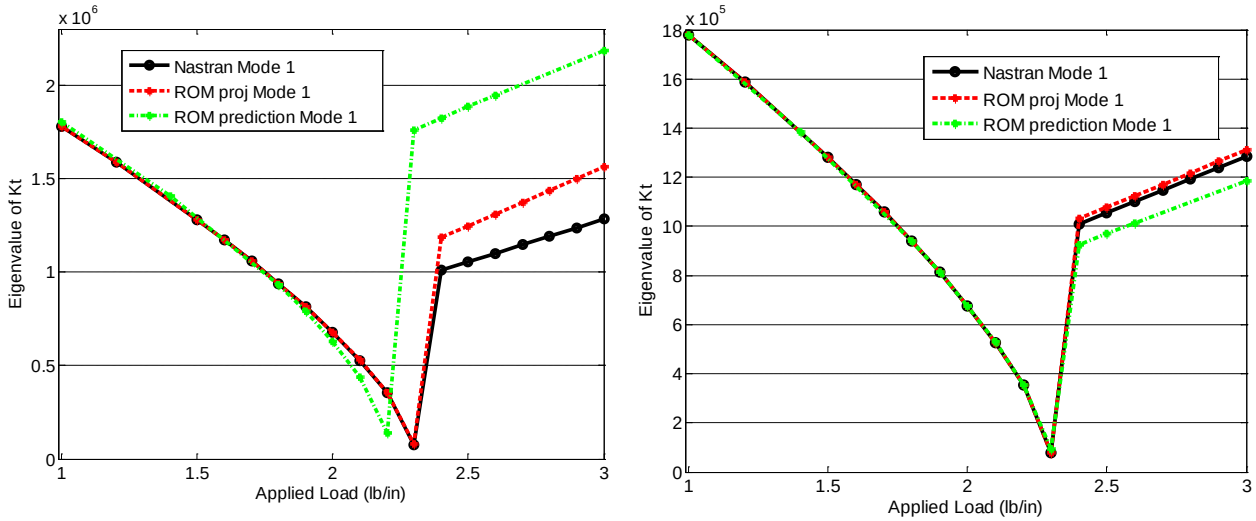

(a) (b)

Figure 9. Lowest eigenvalue of the full Nastran clamped-clamped curved beam model tangent stiffness matrix, of its projection on the ROM basis, and of the ROM, all as functions of the magnitude of the uniform applied load. (a) ROM 4L4D (b) ROM 6L7D

IV. ROM Application to Joined Wings

Two versions of the PrandtlPlane general wing configuration of Fig. 2 were considered here, i.e. the unswept and swept models of Fig. 10. They correspond to Fig. 2 with a = 50 mm, b = e = 20 mm, and f = 0 and f =2a for the unswept (Fig. 10(a)) and swept (Fig. 10(b)) models. The thickness was selected as 1mm and the material properties were assumed to be those of aluminum, i.e. Young's modulus of 6.9 10^{10} Pa, Poisson's ratio equal to 0.33, and a density of 2700 kg/m^3. The joined wing was modeled within Nastran with 704 CTRIA elements and 445 nodes and static nonlinear responses were obtained through either SOL 106 or SOL 400.

Before addressing the construction of the reduced order model from the Nastran model, it was of interest to first obtain a preliminary perspective on the wings nonlinear behavior. To this end, different transverse loadings were applied to the upper and lower wings and their nonlinear static deflections were obtained from Nastran SOL 106. In particular, shown in Fig. 11 are the tip deflections of the upper wing due to a downward uniform pressure of constant direction on the upper wing and the bottom wing unloaded. The snap-buckling behavior is clearly seen. A more complete description of the response of these wings is provided in [3].

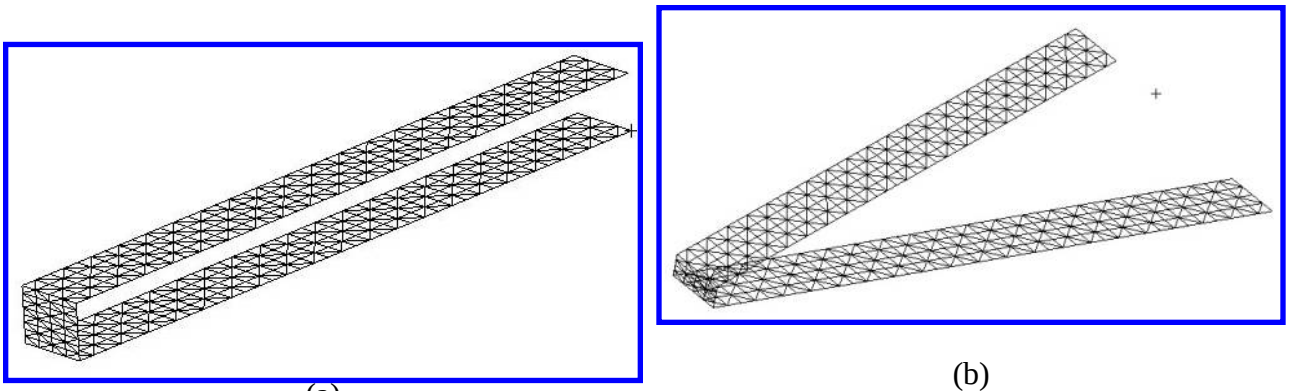

(a) (b)

Figure 10. Finite element models of the PrandtlPlane configurations considered.

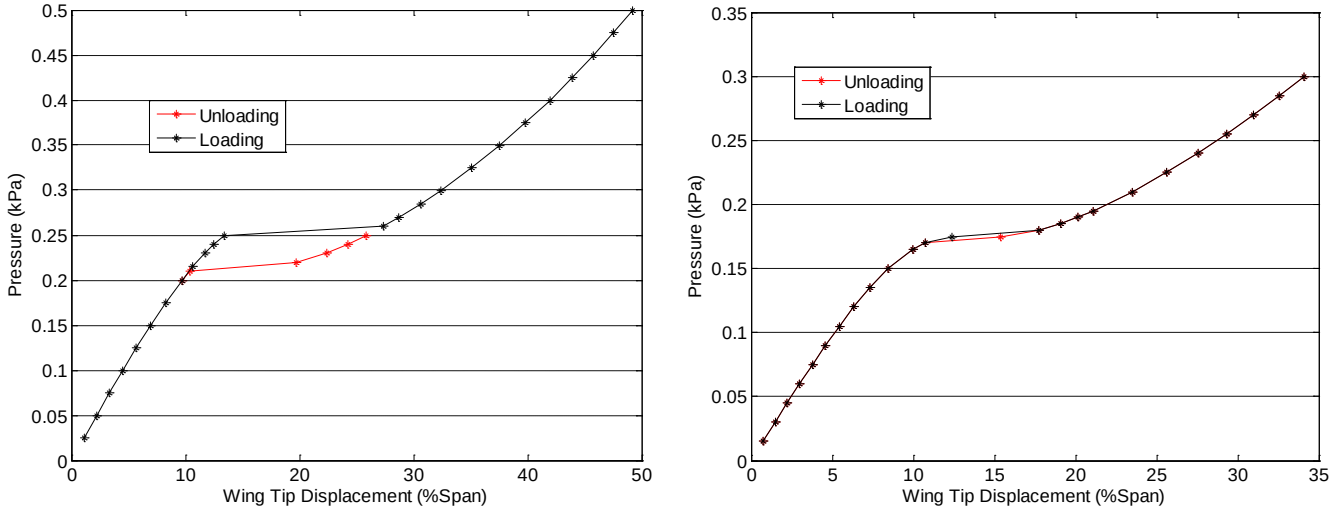

(a) (b)

Figure 11. Load- wing tip displacement behavior. Wings of Fig. 10 with downward uniform pressure on upper wing only.

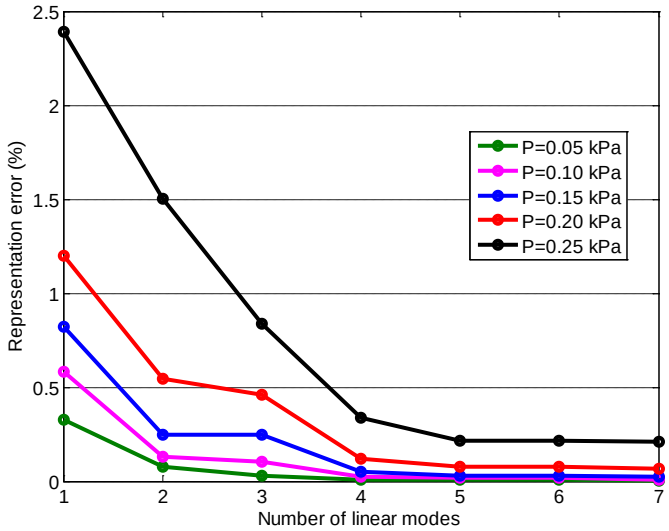

Figure 12. Representation error of the unswept wing, Fig. 10(a), as a function of the number of linear modes for various downward uniform pressures on upper wing only.

Proceeding as in the clamped-clamped curved beam, the first phase of the reduced order model construction was the selection of the basis. The unswept model of Fig. 10(a) was considered first and the number of linear modes to select was first investigated. Shown in Fig. 12 is the representation error at different load levels plotted vs. the number of linear modes retained. A rapid convergence of the error is obtained when selecting up to 4 linear modes but is notably slower for a larger number of modes. Accordingly, 4 linear modes were selected.

The next step is the determination of dual modes to be appended to these 4 linear modes. A first attempt to obtaining these duals was carried out using $\alpha_i^{(m)}$ values that led to peak deflections of the wing of approximately 6%, i.e. about 1/2 of the deflection at snap-buckling. This process led to 4 duals and shown in Fig. 13 are the representation errors of the deflections of Fig. 11(a) with this 8-mode model. At first, it would seem that the basis is appropriate, although the error is rapidly increasing in the neighborhood of the snap-buckling load (259Pa). As suggest in the clamped-clamped beam analysis, the analysis of the lowest eigenvalue of the tangent stiffness matrix projected on the basis is quite important and the corresponding first eigenvalue is shown in Fig. 14 vs. its full Nastran predictions. Clearly, the basis is inappropriate. Within this 8-mode model, the eigenvalue *increases* as the load level increases as opposed to decreasing toward zero. Thus, any reduced order model constructed with this basis will be unable to predict the snap-buckling event even though a good representation of the response is achieved, see Fig. 13.

These observations indicated the need to increase the values of $\alpha_i^{(m)}$ to induce larger deflections and thus introduce in the duals the behavior of the wing near its snap-buckling load. This process led to a notable increase in the number of dual modes selected, i.e. 14 vs. the 4 original ones. With the resulting 18-mode basis, the eigenvalue did correctly decrease but did not quite achieve a near zero value. To remedy this situation, the basis was further enriched using the lowest frequency modes around the deformed positions found along the loading path of Fig. 11(a) up to snap-buckling. These modes were projected on the 18-mode basis and their residuals treated in a proper orthogonal decomposition (POD) of which the dominant 4 eigenvectors were retained. The basis thus formed included 22-mode and gave an acceptable lowest eigenvalue near snap-buckling, see Fig. 14, and a very low representation error, see Fig. 15.

A similar process was carried out for the swept wing of Fig. 10(b) and led to a 25-mode model including again 4 linear modes, 10 duals modes, and 11 POD eigenvectors of the first mode residuals. Shown in Figs 16 and 17 are the corresponding representation errors and eigenvalues of the tangent stiffness matrix. Note that the representation error of the first eigenvector is zero owing to the inclusion of the 11 eigenvectors in the basis. This inclusion also led to the near perfect match of the eigenvalue plot of Fig. 17.

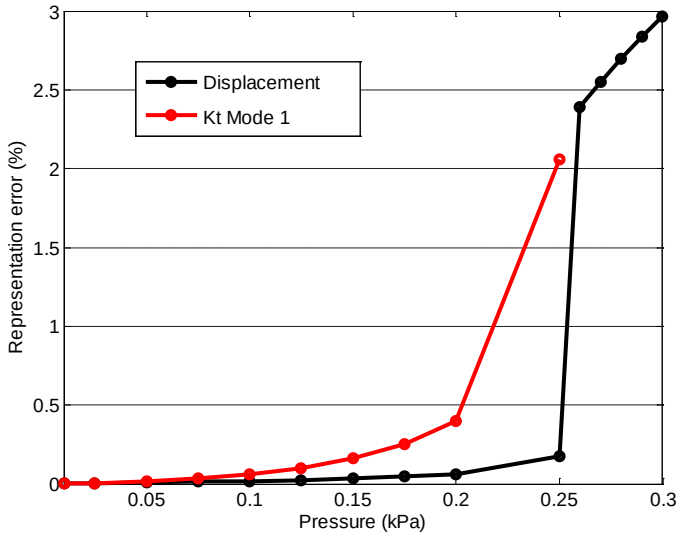

Figure 13. Representation error ε_{rep} of the displacements under downward uniform load on the top wing and of the first eigenvector of the corresponding tangent stiffness matrix, unswept wing, 8-mode model.

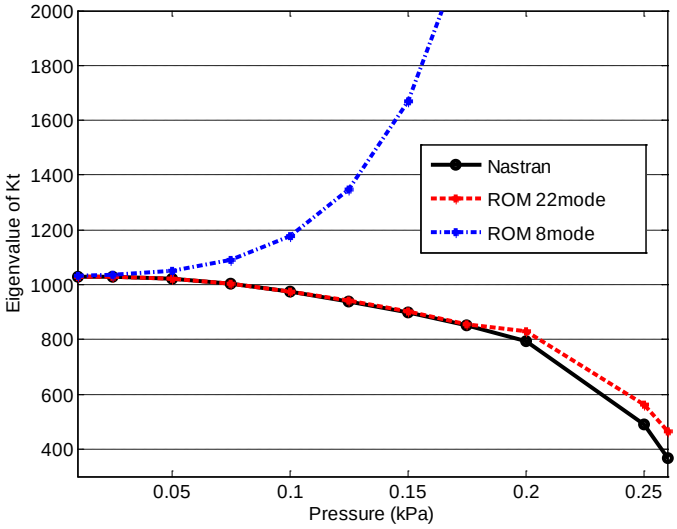

Figure 14. Lowest eigenvalue of the full Nastran unswept wing model tangent stiffness matrix, of its projection on the 8-mode and 22-mode bases as functions of the magnitude of the downward uniform applied load.

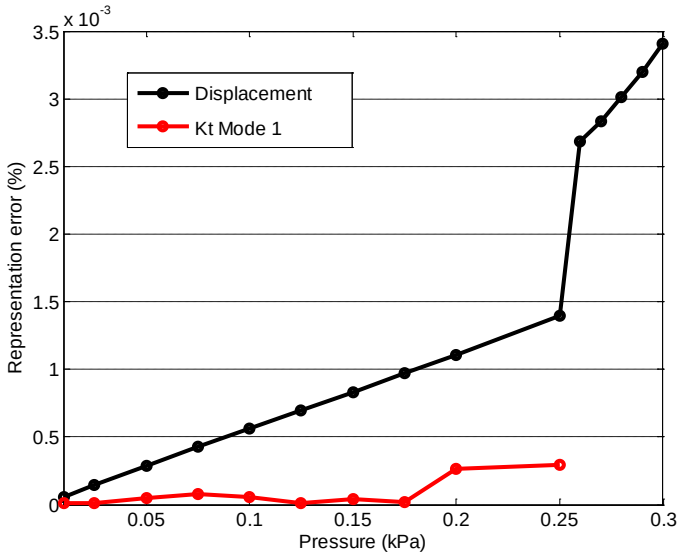

Figure 15. Representation error ε_{rep} of the displacements under downward uniform load on the top wing and of the first eigenvector of the corresponding tangent stiffness matrix, unswept wing, 22-mode model.

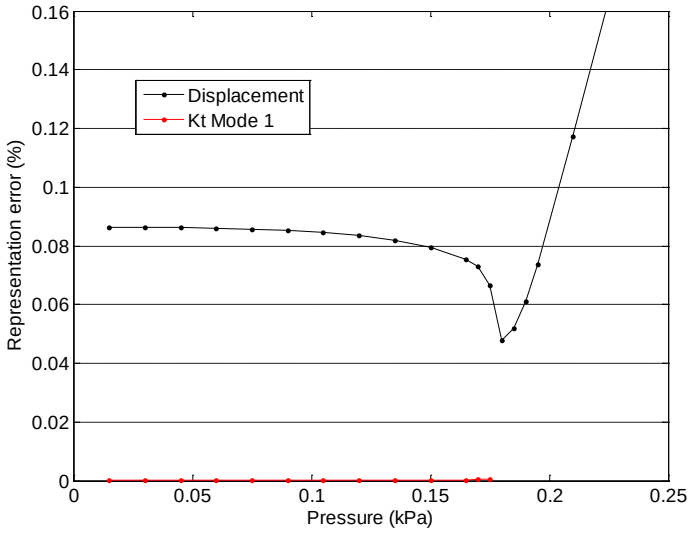

Figure 16. Representation error ε_{rep} of the displacements under downward uniform load on the top wing and of the first eigenvector of the corresponding tangent stiffness matrix, swept wing, 25-mode model.

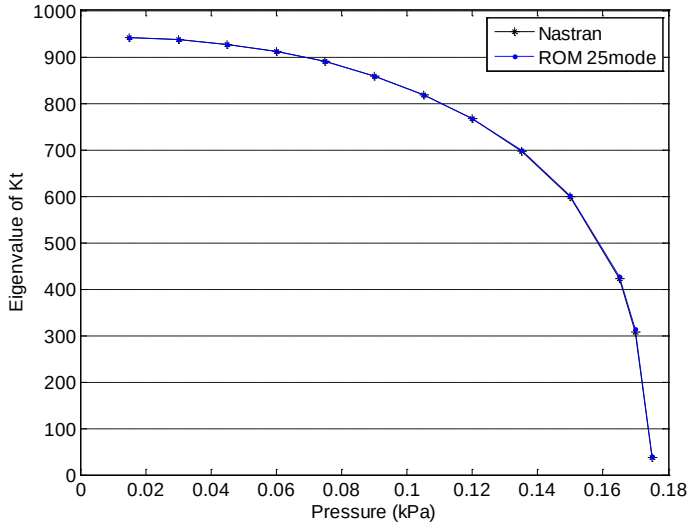

Figure 17. Lowest eigenvalue of the full Nastran swept wing model tangent stiffness matrix and of its projection on the 25-mode bases as functions of the magnitude of the downward uniform applied load.

The above discussion suggests that the 22- and 25- mode bases for the unswept and swept wings should be appropriate for the reduced order modeling of these wings. The next step of the analysis is the identification of the stiffness coefficients which was achieved through both the tangent stiffness and force-displacement approaches described in section II.C. Owing to the difference in the definition of elasticity used in Nastran and in the ROM construction, it has been shown that a subset of these coefficients cannot be accurately determined (e.g. see [8]) and a zeroing out procedure ("coefficient cleaning") has been recommended. This approach was undertaken with the models obtained for the two wings and shown in Figs 18 and 19 are the tip displacements of the wings obtained by Nastran and by the ROMs.

Considering first the unswept wing, it is seen that the ROM captures well the displacement up to the "elbow" of the Nastran curve at which the softening inducing the snap-buckling starts being significant but this ROM does not exhibit the instability. However, extending the cleaning up process to the linear modes 3 and 4 led to a ROM that accurately captured the wing's response just before snap-buckling and led to a buckling but at a slightly higher load than the Nastran model.

The reduced order model of the swept wing, see Fig. 19, matches well the Nastran predicted response and exhibits a softening, albeit somewhat too small, near the snap-buckling. As for the unswept model, buckling is predicted by this model but at a pressure that is too large consistently with the too small softening of the model.

Further investigations of these models are in process to improve the capturing of the buckling event and its ensuing response.

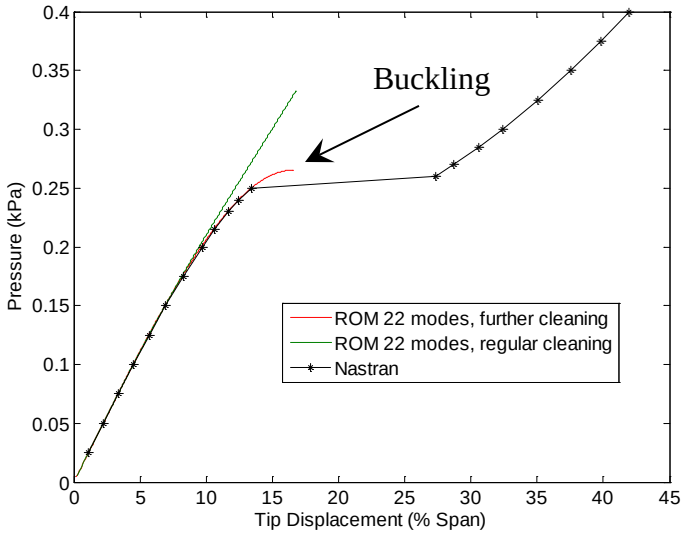

Figure 18. Tip displacement of unswept wing vs. downward uniform pressure on upper wing only. Nastran and ROM predictions.

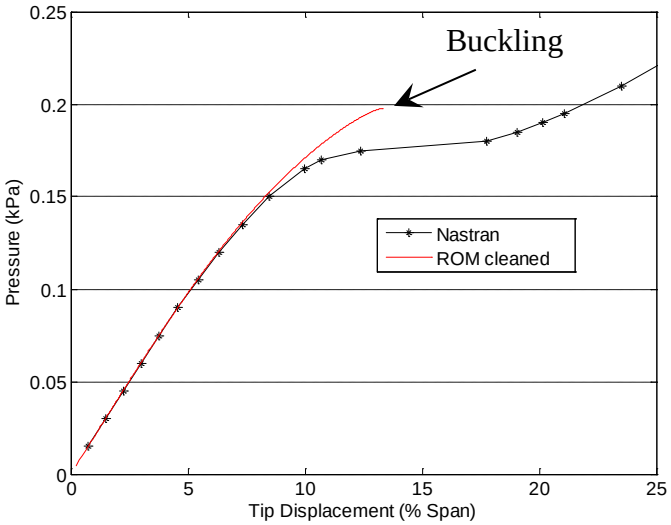

Figure 19. Tip displacement of swept wing vs. downward uniform pressure on upper wing only. Nastran and ROM predictions.

Summary

The focus of this paper was on the extension to joined wings of nonintrusive reduced order modeling techniques of the nonlinear response of structures. Given the complexity of the nonlinear response of these wings, the analysis was carried out in steps through the detailed comparison of the predictions of four different structures: a clamped-clamped plate, a clamped-clamped curved beam, and two examples of joined wings. This effort demonstrated that the reduced order modeling technique is indeed applicable to these wings. A key aspect of this modeling however is the appropriate selection of the basis and new metrics were proposed to evaluate the potential of bases for the prediction of instabilities such as the snap-through of the curved beam or the snap-buckling of the joined wings. Further, the construction of such bases from linear modes and dual modes of the structure, and possibly from eigenvectors of the full finite element tangent stiffness matrix was highlighted. The reduced order models constructed

with such bases performed well to very well in capturing the strongly nonlinear events occurring in the clamped-clamped curved beam and the joined wings.

References

[1] Wolkovitch, J., "The Joined Wing: An Overview," Journal of Aircraft, Vol. 23, No. 3, 1986, pp. 161–178.

[2] Frediani, A., Cipolla, V, and Rizzo, E. "The PrandtlPlane Configuration: Overview on Possible Applications to Civil Aviation" Variational Analysis and Aerospace Engineering: mathematical Challeneges for Aerospace Design, Vol. 66 of Springer Optimization and Its Applications, Springer US, 2012, pp. 179-210, 10.1007/978-1-4614-2435-2_8.[

[3] Demasi L., Cavallaro, R., and Márquez Razón, A., "Postcritical Analysis of PrandtlPlane Joined-Wing Configurations," *AIAA Journal*, Vol. 51, No. 1, pp. 161-177, 2013.

[4] Cavallaro, R., Demasi L., and Passariello, A., "Nonlinear Analysis of PrandtlPlane Joined-Wings – Part II: Effects of Anisotropy" *AIAA 2012-1462*.

[5] Mignolet, M.P., Przekop, A., Rizzi, S.A., and Spottswood, S.M., "A Review of Indirect/Non-Intrusive Reduced Order Modeling of Nonlinear Geometric Structures," *Journal of Sound and Vibration*, Vol. 332, No. 10, pp. 2437-2460, 2013.

[6] Kim, K., Radu, A.G., Wang, X.Q., and Mignolet, M.P., "Nonlinear Reduced Order Modeling of Isotropic and Functionally Graded Plates," *International Journal of Non-Linear Mechanics*, Vol. 49, pp. 100-110, 2013.

[7] Perez, R.A., Wang, X.Q., Matney, A.K., and Mignolet, M.P., "Reduced Order Modeling for the Static and Dynamic Geometric Nonlinear Responses Of a Complex Multi-Bay Structure," *Proceedings of the 11th International Conference on Recent Advances in Structural Dynamics*," Pisa, Italy, Jul. 1-3, 2013.

[8] Wang, X.Q., Perez, R., and Mignolet, M.P., "Nonlinear Reduced Order Modeling of Complex Wing Models," *Proceedings of the 54th Structures, Structural Dynamics and Materials Conference*, Apr. 8-11, 2013, Boston, Massachusetts, AIAA Paper AIAA-2013-1520.

[9] Kim, K., Khanna, V., Wang, X.Q., and Mignolet, M.P., "Nonlinear Reduced Order Modeling of Flat Cantilevered Structures," Proceedings of the 50th Structures, Structural Dynamics, and Materials Conference, Palm Springs, California, May 4-7, 2009. AIAA Paper AIAA-2009-2492.

[10] Spottswood, S.M., Eason, T.G., Wang, X.Q., and Mignolet, M.P., "Nonlinear Reduced Order Modeling of Curved Beams: A Comparison of Methods," Proceedings of the 50th Structures, Structural Dynamics, and Materials Conference, Palm Springs, California, May 4-7, 2009. AIAA Paper AIAA-2009-2433.

[11] Chang, Y.-W., Wang, X.Q., Capiez-Lernout, E., Mignolet, M.P., and Soize, C., "Reduced Order Modeling for the Nonlinear Geometric Response of Some Curved Structures," Proceedings of the 2011 International Forum of Aeroelasticity and Structural Dynamics, Jun. 26-30, 2011, Paris, France, IFASD-2011-185.